R. & M. No. 2994
(17,440)
A.R.C. Technical Report

MINISTRY OF SUPPLY

AERONAUTICAL RESEARCH COUNCIL
REPORTS AND MEMORANDA

Velocities on Two-Dimensional Closed and Semi-Infinite Aerofoils at Zero Incidence

By

S. NEUMARK, Techn.Sc.D., F.R.Ae.S.,
and
B. THWAITES, M.A., Ph.D., A.F.R.Ae.S.

LONDON : HER MAJESTY'S STATIONERY OFFICE
1957
PRICE 4*s* 6*d* NET

Velocities on Two-Dimensional Closed and Semi-Infinite Aerofoils at Zero Incidence

By

S. Neumark, Techn.Sc.D., F.R.Ae.S., and B. Thwaites, M.A., Ph.D., A.F.R.Ae.S.

Communicated by the Principal Director of Scientific Research (Air), Ministry of Supply

Reports and Memoranda No. 2994*

January, 1955

Summary.—An attempt is made to clarify the position as to the comparative two-dimensional velocity distributions on a thin doubly symmetrical aerofoil and on the corresponding semi-infinite body, the front part being the same in the two cases. It is shown that the approximate linear method may be used with advantage to investigate the problem. The method provides a simple general proof that the supervelocity at the mid-chord station of a closed doubly symmetrical profile of any shape is approximately halved when the rear half is replaced by a semi-infinite parallel body. No such simple relationship applies to the entire chordwise distribution on the front part. An exact solution of the velocity distribution has been obtained for one particular semi-infinite profile and several alternative examples have been studied by the linear method. It is found that the ratio of maximum supervelocities may often considerably exceed 0·5 and sometimes rise to nearly 1·0.

1. *Introduction.*—In a recent discussion the question was raised as to the comparative two-dimensional velocity distributions on a thin doubly symmetrical aerofoil and the corresponding semi-infinite body. The purpose of this report is to investigate the matter. It has been found, using the well-known linear perturbation theory of thin symmetric aerofoils, that the value of the supervelocity at mid-chord station on any thin doubly symmetrical aerofoil gets very nearly halved when the rear half is replaced by a semi-infinite parallel body. No such simple rule, however, applies to the entire chord-wise supervelocity distributions in the two cases. At more forward stations, the ratio of corresponding supervelocities may assume values considerably in excess of 0·5, often not much lower than 1. This is shown below not only by general reasoning but also by working out complete velocity distributions by the linear method in several examples, including the biconvex parabolic profile, the ellipse, one very blunt oval, and one oval with particularly thin rounded nose. An exact solution has been found for one semi-infinite profile which is found to have rather exceptional properties in that the maximum supervelocity occurs at mid-chord for both the closed and semi-infinite aerofoil. In many other cases of doubly symmetrical profiles, the maximum may occur not at mid-chord but further upstream, either for the semi-infinite profile, or for both closed and semi-infinite ones.

It is expected that the present note will further emphasize the usefulness of the linear method. It is true that the method is only approximate and that it usually fails in small regions near to stagnation points at leading and trailing edges; it may therefore not appeal to pure mathematicians. It is very useful, however, in many practical applications, and often provides rapid and simple solutions where more rigorous methods would lead to much longer and more elaborate calculations.

An acknowledgement is due to Miss F. M. Ward who has prepared the illustrations.

* R.A.E. Tech. Note Aero. 2362, received 29th April, 1955. This report has been modified to include the results given by Thwaites in A.R.C. 17,158.

2. *General Considerations.*—The linear perturbation method for determining velocity distribution on thin two-dimensional symmetrical aerofoils at zero incidence is well known. It has been discussed in some detail in Ref. 2. It consists in introducing an approximate continuous system of sources and sinks along the chord (Fig. 1a), the local source intensity being proportional to the slope of the profile at the relevant chordwise station. The incremental velocity (supervelocity) at any point P of the profile is calculated approximately as the velocity induced by the source system at the corresponding point A of the chord. If V_∞ denotes the free-stream velocity and V the velocity at P, then the supervelocity is $(V - V_\infty)$, and it is shown in Ref. 2 that this supervelocity can be calculated by the simple formula*:

$$V - \mathrm{V}_\infty = \frac{V_\infty}{\pi} \int \frac{d\bar{y}}{x - \bar{x}}, \qquad \ldots \quad \ldots \quad \ldots \quad \ldots \quad \ldots \quad \ldots \quad (2.1)$$

where the integration must be performed along the entire source-and-sink line LT. The integral is improper, and the principal value must be taken in the usual way. The same formula may be applied to calculate the supervelocity along the x-axis outside the profile, in which case the integral is not improper.

Let us suppose now that the profile is *doubly symmetrical, i.e.,* that, in addition to the symmetry about its chord, it has also fore-and-aft symmetry, as in Fig. 1a. The source-and-sink system is then anti-symmetrical, fore-and-aft, so that every source element S in the front half corresponds to a sink element of the same intensity in the rear half. It is obvious that, at the mid-chord point $\mathrm{P_c}$ (or $\mathrm{A_c}$) the velocities induced by the front and rear halves of the source-and-sink system are exactly equal (and of the same sign).

If we now replace the rear half of the aerofoil by a semi-infinite parallel body (Fig. 1b), the linear theory can still be applied to the resulting *semi-infinite aerofoil* but, as the profile slope in the rear part has become zero, the rear sink system must be simply removed, while the front source system remains as it was in Fig. 1a. The formula (2.1) will still apply, but the integration is to be performed along $\mathrm{LA_c}$ only. It is at once obvious that the supervelocity at $\mathrm{P_c}$ will be half that in the previous case, and this result is quite general, irrespective of the particular shape of the profile. The result is only approximate, of course, but the accuracy should be good for small values of the thickness ratio t/c.

It must be stressed that this simple ratio 0·5 applies only to the mid-chord (maximum thickness) station of doubly-symmetrical profiles. If we consider points on such profiles *further upstream,* the ratio will normally be greater than 0·5, as may be seen again by a simple general reasoning. The supervelocity at any such point (R in Fig. 1a) on the closed profile may again be considered as consisting of two parts, one contributed by the sources, the other one by the sinks. The latter contribution will be generally smaller, however, because the sink elements are at a greater average distance from R than the source elements. In the case of the semi-infinite aerofoil the smaller contribution disappears, and the larger one remains, and hence we may expect the relevant ratio to be anything between 0·5 and 1. This reasoning is perhaps not quite convincing, expecially if we consider points quite near to the leading edge. A considerable part of the source system then induces negative contributions to the supervelocity so that, in most cases, the total supervelocity eventually becomes negative, for both closed and semi-infinite aerofoils (not simultaneously for both). The ratio of supervelocities in the two cases may then assume any positive or negative values, between zero and infinity, but the ratio itself becomes meaningless. In addition, the linear theory generally gives unreliable (sometimes absurd) values very near to the stagnation point at the leading edge. To get a clearer picture of comparative velocity distributions in the two cases, some numerical examples are obviously needed, and these are given in subsequent sections.

---

* There is a slight change in notation from that of Ref. 2, and the positive direction of x-axis has been taken downstream.

The problem may be generalised for *profiles with no fore-and-aft symmetry*. The semi-infinite aerofoil will then be obtained by replacing the rear part of the closed profile behind the maximum thickness station by two parallel tangents at that station. The linear theory will provide velocity distributions in such cases as well (with somewhat more complicated calculations). It is not intended to pursue the matter here, but one remark may be interesting. Suppose that the maximum thickness station of the closed aerofoil is located well forward (*e.g.*, at 20 per cent chord), and the rear part has a very mild slope through most of the remaining chord. The contribution of the sink system to supervelocities on the nose will be very small, and cutting this system off will produce almost no effect.

3. *Exact Solution for a Particular Case (Cycloidal Profile).*—We consider the flow past a particular symmetrical body having a rounded front part faired into two infinite boundaries parallel to the stream, which has a simple hodograph representation (*see* Fig. 2). The maximum supervelocity occurs at the ends of the rounded front part (at P_c and P_c'). It is shown in Appendix I that the parametric equations for the rounded part of the profile are:

$$\left.\begin{aligned} \frac{x}{c} &= \tfrac{1}{2}\sin^2\lambda \\ \frac{y}{c} &= \tfrac{1}{2}(r-1)(\lambda + \sin\lambda\cos\lambda) \end{aligned}\right\} \quad -\frac{\pi}{2} \leqslant \lambda \leqslant \frac{\pi}{2} \qquad (3.1)$$

The maximum velocity is rV_∞, and the thickness ratio is given by:

$$\frac{t}{c} = \tfrac{1}{2}\pi(r-1)\,, \qquad (3.2)$$

where c is the chord of the equivalent closed aerofoil; thus the maximum supervelocity is:

$$V_{\max} - V_\infty = (r-1)V_\infty = \frac{2}{\pi}\frac{t}{c}V_\infty\,, \qquad (3.3)$$

so that, *e.g.*, for $t/c = 0{\cdot}1$, it is $0{\cdot}0637V_\infty$. The maximum supervelocity for the corresponding closed aerofoil has been evaluated by Goldstein's third approximation[1] and found to be $0{\cdot}122V_\infty$. We have therefore, in this particular case:

$$\frac{\text{Maximum supervelocity for the semi-infinite body}}{\text{Maximum supervelocity for the closed aerofoil}} = \frac{0{\cdot}0637V_\infty}{0{\cdot}122V_\infty} = 0{\cdot}522$$

and this differs very little from the simple approximate value $0{\cdot}5$. The exact formulae, in terms of x, for the velocity distribution along the curved front part and also along the straight rear boundary, where $(V - V_\infty)$ is positive but tends to zero when $x \to \infty$, have been found (*see* Appendix I) and are respectively:

$$\frac{V}{V_\infty} = \frac{r}{\sqrt{\left\{1 + (r-1)^2\left(\frac{c}{2x} - 1\right)\right\}}} \qquad (3.4)$$

$$\frac{x}{c} = \frac{r-1}{4}\left[\frac{2(r-1)V_\infty V}{(V - V_\infty)\{rV_\infty - (2-r)V\}} - \ln\frac{rV_\infty - (2-r)V}{r|V - V_\infty|}\right]. \qquad (3.5)$$

This latter formula also applies to the velocity distribution along the x-axis in front of the aerofoil. In the latter case $V < V_\infty$, and that is why the absolute value of $(V - V_\infty)$ is indicated in the second term. The formula cannot be solved explicitly for V, but this does not cause any serious difficulty for computation.

The formulae (3.4) and (3.5) have been used to produce exact curves of velocity distribution for the semi-infinite aerofoil derived from a closed one of thickness ratio 0·1 (*see* Fig. 5). For convenience, the supervelocity ratio $(V - V_\infty)/V_\infty$ has been plotted, as in all subsequent figures.

A striking feature of the graph is the abrupt kink of the curve at P_c, with the vertical tangent to the right-hand part of the curve. This feature suggests a violent discontinuity of curvature at P_c which seems puzzling: the thickness ratio being small, one would expect a very small curvature of the profile at P_c. The curvature is 0, of course, on the straight boundary downstream, so the discontinuity is there without doubt, but the shape of the curve still seems surprising. The matter is easily explained, however, if we calculate the radius of curvature of the profile exactly. The formula is:

$$\varrho = \frac{\pi}{2}\frac{c^2}{t}\sin^3\lambda\cos\lambda\left(1+\frac{4}{\pi^2}\frac{t^2}{c^2}\cot^2\lambda\right)^{3/2}, \qquad \ldots\ \ldots\ \ldots\ \ldots \quad (3.6)$$

and hence *at P_c (where $x = 0{\cdot}5c$; $\lambda = \pi/2$) the radius of curvature is zero, and the curvature infinite!* This seems preposterous but is perfectly correct. The fact that the profile seems to have a very feeble curvature at P_c may be explained by calculating ϱ very near to P_c. It is easily found that, if t/c is small, then:

$$\text{for } x = 0{\cdot}495c, \text{ we have } \cos\lambda = 0{\cdot}1\,, \quad \varrho \simeq 0{\cdot}155c^2/t\,,$$

$$\text{for } x = 0{\cdot}48c, \text{ we have } \cos\lambda = 0{\cdot}2\,, \quad \varrho \simeq 0{\cdot}293c^2/t\,, \text{ etc.},$$

so that the radius of curvature becomes quite large at very small distances from P_c.

This geometrical singularity of our curve is a very unusual thing for a wing profile, but is nothing new in mathematics. The same sort of singularity occurs at cusps of many elementary curves, *e.g.*, of a semi-cubic parabola, or of an ordinary cycloid. Now, it is easily found that, if λ is varied from $(-\infty)$ to $(+\infty)$ in equations (3.1), we obtain a curve (Fig. 3) consisting of an infinite number of identical branches, with an infinite number of cusps, very similar to a cycloid. And, in the special case $r = 2$, our curve actually becomes a cycloid, the equations becoming then:

$$x = \tfrac{1}{4}c(1 - \cos 2\lambda)\,, \qquad y = \tfrac{1}{4}c(2\lambda + \sin 2\lambda)\,. \quad \ldots\ \ldots\ \ldots\ \ldots \quad (3.7)$$

If r is given any alternative value (which will be only little in excess of 1 if the thickness ratio is to be small), the ordinates y are simply scaled down, and we obtain curves 'affine' to the cycloid.

4. *Cycloidal Profile Treated by Linear Method.*—It is interesting to find the supervelocity on the cycloidal semi-infinite aerofoil by applying the linear approximation, *i.e.*, the formula (2.1). As shown in Appendix II, the result is:

$$\frac{V - V_\infty}{V_\infty} = r - 1 = \frac{2}{\pi}\frac{t}{c}, \qquad (0 < x < \tfrac{1}{2}c)\ \ldots\ \ldots\ \ldots\ \ldots\ \ldots \quad (4.1)$$

and

$$\frac{V - V_\infty}{V_\infty} = (r-1)\left[1 - \sqrt{\left(1 - \frac{c}{2x}\right)}\right], \qquad (x > \tfrac{1}{2}c, \text{ or } x < 0)\ \ldots\ \ldots \quad (4.2)$$

The formula (4.1) gives, somewhat surprisingly, a constant supervelocity along the entire curved front part of the aerofoil, the value being, however, the same as the exact maximum obtained by the rigorous method (*see* 3.3). This result becomes understandable when we examine the exact formula (3.4). The factor $(r - 1)^2$ being small of the second order in terms of thickness ratio, the expression (3.4) differs from r only by a small term of the second order, except near the leading edge where the difference assumes increasingly large values. Our result is therefore consistent with the assumptions of the linear theory.

The formula (4.2) applies for both $x > \frac{1}{2}c$ and $x < 0$, and gives the supervelocity on the straight boundary of the semi-infinite aerofoil, and on the x-axis in front of it, respectively. The results are plotted again in Fig. 5 for the case $t/c = 0{\cdot}1$, and marked ' lin. approx.'. It will be noted that, for $x > \frac{1}{2}c$, the approximate curve lies so close to the exact one that the differences cannot be seen on the scale adopted. For $x < 0$, the differences are only just visible.

The linear method can also be applied to the *closed profile* and, in view of the fore-and-aft symmetry, the curves can be drawn at once, by simply adding the ordinates of the previous curves corresponding to x and $(c - x)$, respectively. The formulae in this case are:

$$\left.\begin{aligned} \frac{V - V_\infty}{V_\infty} &= (r-1)[2 - \sqrt{\{1 - c/(2c - 2x)\}}] && \left(0 < x < \frac{c}{2}\right) \\ &= (r-1)[2 - \sqrt{\{1 - c/2x\}}] && \left(\frac{c}{2} < x < c\right) \\ &= (r-1)[2 - \sqrt{\{1 - c/2x\}} - \sqrt{\{1 - c/(2c - 2x)\}}] && (x > c, \text{ or } x < 0) \end{aligned}\right\} . \quad (4.3)$$

The curves have also been traced in Fig. 5, and it is seen that there is a true cusp at the mid-chord station. An alternative curve for the closed aerofoil, marked ' almost exact ', is also shown, as obtained by adding the ordinates of the exact curve referring to the semi-infinite body, which correspond to x and $(c - x)$, respectively. This procedure is still not perfectly exact, but errors should be very small, in particular in the region near the stagnation points.

The cusp at mid-chord station is a very unusual feature in a velocity graph. It is obviously due to the geometrical singularity of the profile described in the previous section. From this point of view, our example would not perhaps be very fortunate if a comparison with experiment were required. The point is that it would be extremely difficult to manufacture a thin model with such an accuracy as to have really zero radius of curvature at maximum thickness, and experimental pressure plotting would probably never reveal a true cusp. Irrespective of this difficulty, Fig. 5 shows clearly that the ratio of supervelocities on the semi-infinite and closed aerofoil equals $0{\cdot}5$ only at mid-chord station, while it assumes considerably higher values further upstream (*e.g.*, about $0{\cdot}75$ at $x = 0{\cdot}1c$). The ratio $0{\cdot}5$ applies, however, to maximum supervelocities, as these happen to occur at mid-chord station for both aerofoils. This feature is rather unusual, as will be shown by alternative examples.

5. *Alternative Example : Biconvex Parabolic Profile.*—For the biconvex parabolic profile (Fig. 6) the linear method gives particularly simple solutions. It is more convenient in this case to place the origin of co-ordinates at mid-chord. The equation of the profile is then:

$$y = \tfrac{1}{2}t(1 - \xi^2), \text{ where } \xi = 2x/c \quad .. \quad .. \quad .. \quad .. \quad .. \quad .. \quad .. \quad (5.1)$$

and, as shown in Appendix III, the supervelocities on the semi-infinite and closed aerofoil are given, respectively, by the following formulae:

$$\frac{V - V_\infty}{V_\infty} = \frac{2}{\pi}\frac{t}{c}\left\{1 - \xi \ln\left|\frac{1+\xi}{\xi}\right|\right\} \quad \text{(semi-infinite)} \quad .. \quad .. \quad .. \quad .. \quad .. \quad .. \quad (5.2)$$

$$\frac{V - V_\infty}{V_\infty} = \frac{4}{\pi}\cdot\frac{t}{c}\left\{1 - \tfrac{1}{2}\xi \ln\left|\frac{1+\xi}{1-\xi}\right|\right\} \text{ (closed) .} \quad .. \quad .. \quad .. \quad .. \quad .. \quad .. \quad (5.3)$$

Both formulae apply throughout the entire range of ξ from $(-\infty)$ to $(+\infty)$, the straight brackets being used to denote the absolute value. A graphical illustration is given in Fig. 6, for thickness ratio $0{\cdot}1$.

The ratio of supervelocities in the two cases is, of course, $0\cdot5$ at $\xi = 0$, and the respective values are, curiously enough, exactly equal to those found previously for the cycloidal profile. However, only for the closed profile does the maximum occur at mid-chord station. For the semi-infinite aerofoil, the curve presents a vertical inflexion tangent at $\xi = 0$ (effect of discontinuity of curvature), and the maximum value, at about $\xi = -0\cdot218$, amounts to about $0\cdot64$ of that for the closed profile. The ratio of corresponding supervelocities further upstream from mid-chord station increases from $0\cdot5$ to about $0\cdot7$ (at $\xi \doteq -0\cdot4$). All these numerical results are only approximate but the accuracy is certainly good enough.

6. *Further Examples : Oval Profiles, including Ellipse.*—A family of oval profiles was considered in Ref. 2 (Appendix I, example VI, Fig. 19), the equation being:

$$y = \tfrac{1}{2}t(1-\xi^2)^{1/2}\,(1+k\xi^2)\ ,\ \text{with}\ \xi = 2x/c \qquad .. \quad .. \quad .. \quad .. \quad .. \quad .. \quad (6.1)$$

where k is a variable parameter. If $k = 0$, this represents an ellipse; for k increasingly positive, the profile becomes fuller (Fig. 9), and for k increasingly negative we obtain profiles with gradually thinner noses (Fig. 7). The supervelocities on both semi-infinite and closed aerofoils are derived by linear method in Appendix IV. The formulae are somewhat complicated but simplify considerably for the elliptic profile, for which we obtain:

(*a*) *Semi-infinite aerofoil with elliptic front part :*

$$\frac{V-V_\infty}{V_\infty} = \frac{t}{2c}\left\{1 - \frac{\xi}{\pi\sqrt{(1-\xi^2)}}\ln\frac{1+\sqrt{(1-\xi^2)}}{1-\sqrt{(1-\xi^2)}}\right\}, \qquad (\xi^2<1) \qquad .. \quad .. \quad (6.2a)$$

$$= \frac{t}{2c}\left\{1 - \frac{4}{\pi}\left(\frac{\xi^2}{\xi^2-1}\right)^{1/2}\tan^{-1}\sqrt{\left(\frac{\xi-1}{\xi+1}\right)}\right\}; \qquad (\xi^2>1) \qquad .. \quad .. \quad (6.2b)$$

(*b*) *Closed elliptic aerofoil:*

$$\frac{V-V_\infty}{V_\infty} = \frac{t}{c}, \qquad (\xi^2<1) \qquad .. \quad .. \quad (6.3a)$$

$$= \frac{t}{c}\left\{1 - \sqrt{\left(\frac{\xi^2}{\xi^2-1}\right)}\right\}. \qquad (\xi^2>1) \qquad .. \quad .. \quad (6.3b)$$

Illustrative graphs, for thickness ratio $0\cdot1$, are given in Fig. 8. At $\xi = 0$, there is again a vertical inflexion tangent for the semi-infinite aerofoil. The drop in supervelocity is, however, less abrupt than in the previous cases, and this is understandable as the radius of curvature of the ellipse, at $\xi = 0$, is comparatively large ($0\cdot5c^2/t$, as against $0\cdot25c^2/t$ for the parabolic profile, and 0 for the cycloidal profile).

The constant value obtained by the linear method for the closed ellipse is a well known result[2]. The exact velocity distribution on an elliptic profile (and along the x-axis in front and behind the profile) is easily obtained by conformal transformation:

$$\frac{V-V_\infty}{V_\infty} = \left(1+\frac{t}{c}\right)\sqrt{\left(\frac{1-\xi^2}{1-(1-t^2/c^2)\xi^2}\right)} - 1\ , \qquad (\xi^2<1) \qquad .. \quad .. \quad (6.4a)$$

$$= \frac{t/c}{1-t/c}\left\{1 - \sqrt{\left(\frac{\xi^2}{\xi^2-1+t^2/c^2}\right)}\right\}, \qquad (\xi^2>1) \qquad .. \quad .. \quad (6.4b)$$

and the illustrative curves are also given in Fig. 8. The differences between (6.3a) and (6.4a) are small of second order in t/c, except near the stagnation points. An ' almost exact ' curve for the semi-infinite aerofoil has been obtained from the approximate one, by decreasing its ordinates by the corresponding differences between those of the exact and approximate curves referring to the closed ellipse.

It is seen again that the ratio of supervelocities in the two cases becomes considerably larger than 0·5 on the front half of the profile, reaching the value about 0·78 at $\xi = -0{\cdot}7$. The ratio of maxima is nearly 0·75.

It is interesting to compare Figs. 5 and 8 (cycloidal and elliptic profile). There are considerable differences in supervelocity curves, although the two profiles seem so similar. The true difference between the profiles can be better appreciated in Fig. 4, where the ordinates are scaled up to thickness ratio 1.

Further illustrative graphs are presented in Figs. 7 and 9 for two oval profiles of the type (6.1). They have been calculated from the formulae given in Appendix IV (linear method only). In Fig. 7, $k = -0{\cdot}4$, and we have a thin-nosed profile (still with a rounded edge). The supervelocity curves are rather similar to those of Fig. 6 along major parts of the chords, but differences are considerable near stagnation points where the accuracy is poor anyhow. It may be noted that the radii of curvature of the two profiles at $\xi = 0$ are nearly equal ($0{\cdot}25c^2/t$ in Fig. 6, $0{\cdot}278c^2/t$ in Fig. 7). Fig. 9 refers to a rather extreme case of a very full blunt profile ($k = +0{\cdot}4$). The radius of curvature at $\xi = 0$ amounts to as high a value as $2{\cdot}5c^2/t$, and this accounts for the fact that the singularity of the velocity curve for the semi-infinite aerofoil is almost invisible—a vertical inflection tangent is, however, still there. The supervelocities in the front part of the profile rise to very high values for both semi-infinite and closed aerofoils, and the true maxima must occur not far from the leading edge. The errors must be large in this region. There is no doubt, however, that the ratio of supervelocities in the two cases must rise to remarkably high values—about 0·85 or 0·9 for the maxima.

REFERENCES

No.	*Author*	*Title, etc.*
1	S. Goldstein	Approximate two-dimensional aerofoil theory. Part I: Velocity distributions for symmetrical aerofoils. C.P. 68. May, 1942.
2	S. Neumark	Velocity distribution on straight and swept-back wings of small thickness and infinite aspect ratio at zero-incidence. R. & M. No. 2713. May, 1947.

APPENDIX I

Derivation of some Exact Formulae Pertaining to the Cycloidal Profile (*Section* 3)

To derive the exact solution for a semi-infinite aerofoil, let us consider the hodograph plane (Fig. 2), where the interior of the circle

$$|\zeta - \tfrac{1}{2}rV_\infty| = \tfrac{1}{2}rV_\infty$$

corresponds to the exterior of the aerofoil in the physical plane. The complex potential $w = \phi + i\psi$ has been expressed in terms of $\zeta = V_x - iV_y$ by the relationship:

$$w = \phi + i\psi = M\left[\frac{1}{\zeta - V_\infty} - \frac{r^2}{2-r}\frac{1}{(2-r)\zeta - rV_\infty}\right], \quad .. \quad .. \quad \text{(I.1)}$$

which represents a doublet of strength M at $\zeta = V_\infty$ together with its image at $\zeta = rV_\infty/(2-r)$. Values on OP_c are:

$$\left.\begin{aligned} &\psi = 0\,, \quad w = \phi \\ &\zeta = rV_\infty \cos\theta \,.\, e^{-i\theta} = \frac{dw}{dz} = e^{-i\theta}\frac{d\phi}{ds} \end{aligned}\right\} \quad .. \quad .. \quad .. \quad .. \quad \text{(I.2)}$$

(4626) A**

and so

$$ds = \frac{1}{rV_\infty} \sec\theta \, d\phi \,, \qquad \text{(I.3)}$$

whence

$$\left.\begin{aligned} dx &= \frac{d\phi}{rV_\infty} \\ dy &= \frac{\tan\theta \, d\phi}{rV_\infty} \end{aligned}\right\} \qquad \text{(I.4)}$$

Substituting the value for ζ from (I.2) into (I.1), we find

$$\phi = \frac{2M}{V_\infty} \frac{r-1}{2-r} \frac{1+\tan^2\theta}{(r-1)^2+\tan^2\theta} \qquad \text{(I.5)}$$

and, if

$$\tan\theta = (r-1)\cot\lambda \qquad \text{(I.6)}$$

this becomes:

$$\phi = \frac{2M}{V_\infty} \frac{\sin^2\lambda + (r-1)^2\cos^2\lambda}{(r-1)(2-r)} \,. \qquad \text{(I.7)}$$

The geometric scale may now be fixed by putting $4M = c(r-1)V_\infty{}^2$, c being the chord of the corresponding doubly symmetrical aerofoil. Using (I.7) to integrate (I.4) we then obtain the parametric equations of the curved front part of the semi-infinite aerofoil:

$$\left.\begin{aligned} x &= \tfrac{1}{2}\sin^2\lambda \\ y &= \tfrac{1}{2}(r-1)(\lambda + \tfrac{1}{2}\sin 2\lambda) \end{aligned}\right\} \quad -\frac{\pi}{2} \leqslant \lambda \leqslant \frac{\pi}{2} \,. \qquad \text{(I.8)}$$

The formulae for the velocity $V = d\phi/ds$ along OP_c is found from (I.3) and (I.6), and we obtain:

$$\frac{V}{V_\infty} = r[1 + (r-1)^2\cot^2\lambda]^{-1/2} \qquad \text{(I.9)}$$

or, in terms of x:

$$\frac{V}{V_\infty} = \frac{r}{\sqrt{\left\{1 + (r-1)^2\left(\frac{c}{2x} - 1\right)\right\}}} \,. \qquad \text{(I.10)}$$

A similar method can be applied to determine velocity distribution along P_cQ or SO. In both cases $V_y = 0$, $\zeta = V$ and $\psi = 0$, $w = \phi$, so that:

$$\phi = M\left[\frac{1}{V - V_\infty} - \frac{r^2}{2-r}\frac{1}{(2-r)V - rV_\infty}\right] \,. \qquad \text{(I.11)}$$

Differentiating (I.11) with respect to x and noting that $d\phi/dx = V$, we obtain the following differential equation with separated variables V and x:

$$\frac{dx}{M} = \left[\frac{r^2}{V\{(2-r)^2V - rV_\infty\}^2} - \frac{1}{V(V - V_\infty)^2}\right] dV \,. \qquad \text{(I.12)}$$

This equation must be integrated separately along P_cQ (where $V_\infty < V < V_\infty r$, and the constant of integration must be determined so that $V = V_\infty r$ for $x = \frac{1}{2}c$) and along SO (where $0 < V < V_\infty$, and $V = 0$ for $x = 0$). It is easily found that the formula (3.5) applies on both P_cQ and SO, provided the absolute value of $(V - V_\infty)$ is always taken in the second term.

APPENDIX II

Derivation of Formulae for Cycloidal Profile by Linear Method (Section 4)

Applying (2.1) and (3.1), we obtain for the semi-infinite aerofoil:

$$\frac{V - V_\infty}{V_\infty} = \frac{1}{\pi}\int_{\bar{x}=0}^{\frac{1}{2}c} \frac{d\bar{y}}{x - \bar{x}} = \frac{r-1}{\pi}\int_0^{\frac{1}{2}\pi} \frac{1 + \cos 2\bar{\lambda}}{2(x/c) - \sin^2 \bar{\lambda}}\, d\bar{\lambda}$$

$$= \frac{r-1}{\pi}\int_0^{\pi}\left(1 + \frac{2 - 4(x/c)}{4(x/c) - 1 + \cos 2\bar{\lambda}}\right) d(2\bar{\lambda}) \,. \quad .. \quad .. \quad .. \quad \text{(II.1)}$$

The integral of the second term is improper and easily found to be equal to 0 when $|4(x/c) - 1| < 1$; it is not improper and equal to $\pi\sqrt{(1 - c/2x)}$ when $|4(x/c) - 1| > 1$. This leads directly to (4.1) and (4.2).

APPENDIX III

Derivation of Formulae for Biconvex Parabolic Profile (Section 5)

Applying (2.1) and (5.1), we obtain for the semi-infinite aerofoil:

$$\frac{V - V_\infty}{V_\infty} = -\frac{2t}{\pi c}\int_{-1}^{0} \frac{\bar{\xi}\, d\bar{\xi}}{\xi - \bar{\xi}} = \frac{2t}{\pi c}\int_{-1}^{0}\left(1 - \frac{\xi}{\xi - \bar{\xi}}\right) d\bar{\xi} \,. \quad .. \quad .. \quad .. \quad \text{(III.1)}$$

The integral of the second term is improper if $-1 < \xi < 0$, and not improper for $\xi > 0$ or $\xi < -1$. The formula (5.2) is obtained in all cases.

For the closed aerofoil, the upper limit of integration in (III.1) must be changed to $(+1)$, and the integral will be improper when $|\xi| < 1$. In all cases the formula (5.3) will be found to apply.

APPENDIX IV

Derivation of Formulae for Oval Profiles, including Ellipse (Section 6)

Applying (2.1) and (6.1), we obtain for the semi-infinite aerofoil:

$$\frac{V - V_\infty}{V_\infty} = -\frac{t}{\pi c}\int_{-1}^{0} \frac{\bar{\xi}(1 - 2k + 3k\bar{\xi}^2)}{(\xi - \bar{\xi})\sqrt{(1 - \bar{\xi}^2)}}\, d\bar{\xi} \,. \quad .. \quad .. \quad .. \quad .. \quad \text{(IV.1)}$$

Substituting

$$\bar{\xi} = \sin\bar{\omega} \,, \quad .. \quad .. \quad .. \quad .. \quad .. \quad .. \quad .. \quad .. \quad \text{(IV.2)}$$

we may write (IV.1) as follows:

$$\frac{V - V_\infty}{V_\infty} = \frac{t}{\pi c}\int_{-\frac{1}{2}\pi}^{0} \frac{3k\sin^3\bar{\omega} + (1 - 2k)\sin\bar{\omega}}{\sin\bar{\omega} - \xi}\, d\bar{\omega}$$

$$= \frac{t}{\pi c}\int_{-\frac{1}{2}\pi}^{0}\left[3k\sin^2\bar{\omega} + 3k\xi\sin\bar{\omega} + (1 - 2k + 3k\xi^2) + \frac{\xi(1 - 2k + 3k\xi^2)}{\sin\bar{\omega} - \xi}\right] d\bar{\omega} \,. \quad \text{(IV.3)}$$

For the closed aerofoil the same formula (IV.3) will apply, with the upper limit of integration changed to $(+\frac{1}{2}\pi)$.

The first three terms in (IV.3) are easily integrated. The fourth integral will assume three different forms for various intervals of ξ, *viz.*:

$$\left.\begin{aligned}\int_{-\frac{1}{2}\pi}^{0}\frac{d\bar{\omega}}{\sin\bar{\omega}-\xi} &= -\frac{1}{2\sqrt{(1-\xi^2)}}\ln\frac{1+\sqrt{(1-\xi^2)}}{1-\sqrt{(1-\xi^2)}} && (\xi^2<1)\,,\\ &= -\frac{2}{\sqrt{(\xi^2-1)}}\tan^{-1}\sqrt{\left(\frac{\xi-1}{\xi+1}\right)} && (\xi>1)\,,\\ &= +\frac{2}{\sqrt{(\xi^2-1)}}\tan^{-1}\sqrt{\left(\frac{-\xi+1}{-\xi-1}\right)} && (\xi<-1)\end{aligned}\right\} \quad \ldots\ \ldots \text{(IV.4)}$$

and

$$\left.\begin{aligned}\int_{-\frac{1}{2}\pi}^{\frac{1}{2}\pi}\frac{d\bar{\omega}}{\sin\bar{\omega}-\xi} &= 0 && (\xi^2<1)\,,\\ &= -\frac{\pi}{\sqrt{(\xi^2-1)}} && (\xi>1)\,,\\ &= +\frac{\pi}{\sqrt{(\xi^2-1)}} && (\xi<-1)\,.\end{aligned}\right\} \quad \ldots\ \ldots \text{(IV.5)}$$

Using (IV.4) and (IV.5), we finally obtain:

for the semi-infinite aerofoil:

$$\left.\begin{aligned}\frac{V-V_\infty}{V_\infty} &= \frac{t}{c}\left[\left(\tfrac{1}{2}-\frac{k}{4}\right)-\frac{3k}{\pi}\xi\right.\\ &\quad \left.+\frac{3k}{2}\xi^2-\frac{\xi(1-2k+3k\xi^2)}{2\pi\sqrt{(1-\xi^2)}}\ln\frac{1+\sqrt{(1-\xi^2)}}{1-\sqrt{(1-\xi^2)}}\right] && (\xi^2<1)\,,\\ &= \frac{t}{c}\left[\left(\tfrac{1}{2}-\frac{k}{4}\right)-\frac{3k}{\pi}\xi\right.\\ &\quad \left.+\frac{3k}{2}\xi^2-\frac{2(1-2k+3k\xi^2)}{\pi}\left(\frac{\xi^2}{\xi^2-1}\right)^{1/2}\tan^{-1}\sqrt{\left(\frac{\xi-1}{\xi+1}\right)}\right] && (\xi^2>1)\,,\end{aligned}\right\}; \quad \text{(IV.6)}$$

and for the closed one :

$$\left.\begin{aligned}\frac{V-V_\infty}{V_\infty} &= \frac{t}{c}(1-\tfrac{1}{2}k+3k\xi^2) && (\xi^2<1)\,,\\ &= \frac{t}{c}\left[1-\tfrac{1}{2}k+3k\xi^2-(1-2k+3k\xi^2)\sqrt{\left(\frac{\xi^2}{\xi^2-1}\right)}\right]. && (\xi^2>1)\,.\end{aligned}\right\} \quad \text{(IV.7)}$$

The formulae (6.2) and (6.3) are particular cases of (IV.6) and (IV.7), for $k=0$.

It may be mentioned that the first derivative of (IV.6) becomes logarithmically infinite for $\xi=0$, and hence the supervelocity curves for the semi-infinite aerofoils in Figs. 7, 8 and 9 have vertical inflexion tangents at mid-chord station, in agreement with the fact that there is a discontinuity of curvature there. An exceptional case occurs, however, when $k=0{\cdot}5$, for which value the first derivative becomes finite at $\xi=0$. It is easily found that the radius of curvature of any oval profile of our family, at $\xi=0$, is expressed by the simple formula:

$$\varrho_{\xi=0}=c^2/2t(1-2k)\,, \quad \ldots\ \ldots\ \ldots\ \ldots\ \ldots\ \ldots\ \ldots\ \ldots \text{(IV.8)}$$

so that it becomes ∞ for $k=0{\cdot}5$. When k increases beyond $0{\cdot}5$, the ovals acquire a waist in the middle, and the problem is of no practical significance.

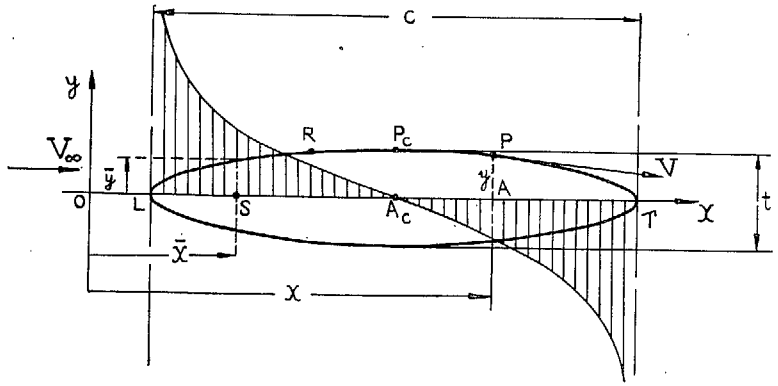

FIG. 1a. Sources distribution for a closed doubly symmetrical aerofoil.

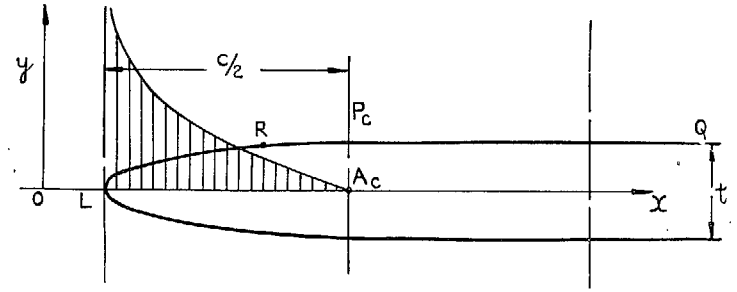

FIG. 1b. Sources distribution for a semi-infinite aerofoil.

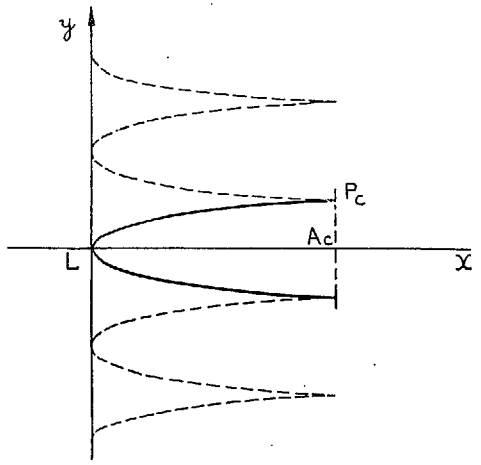

FIG. 3. Cycloidal profile as a branch of a curve affine to a cycloid.

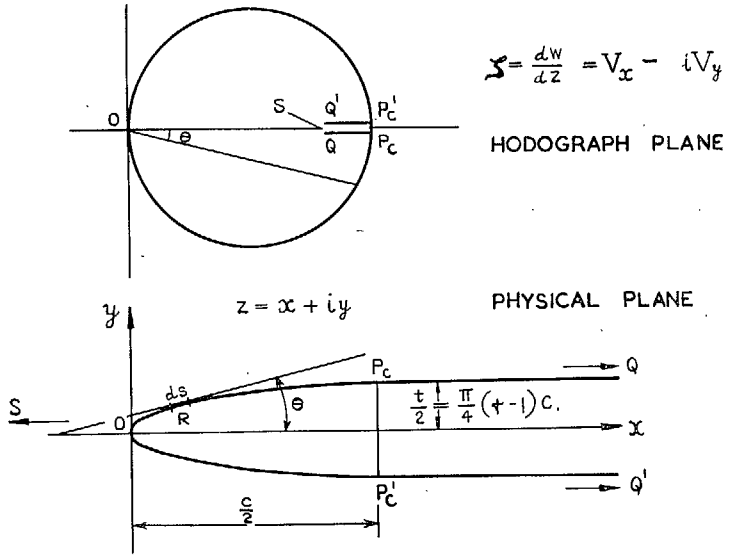

FIG. 2. Hodograph plane and physical plane for cycloidal profile.

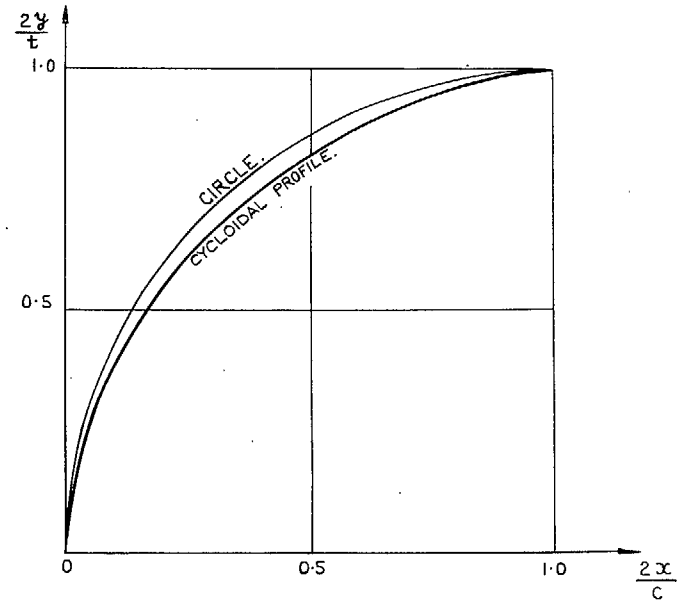

FIG. 4. Comparison of cycloidal profile with an ellipse, scaled up to thickness ratio 1.

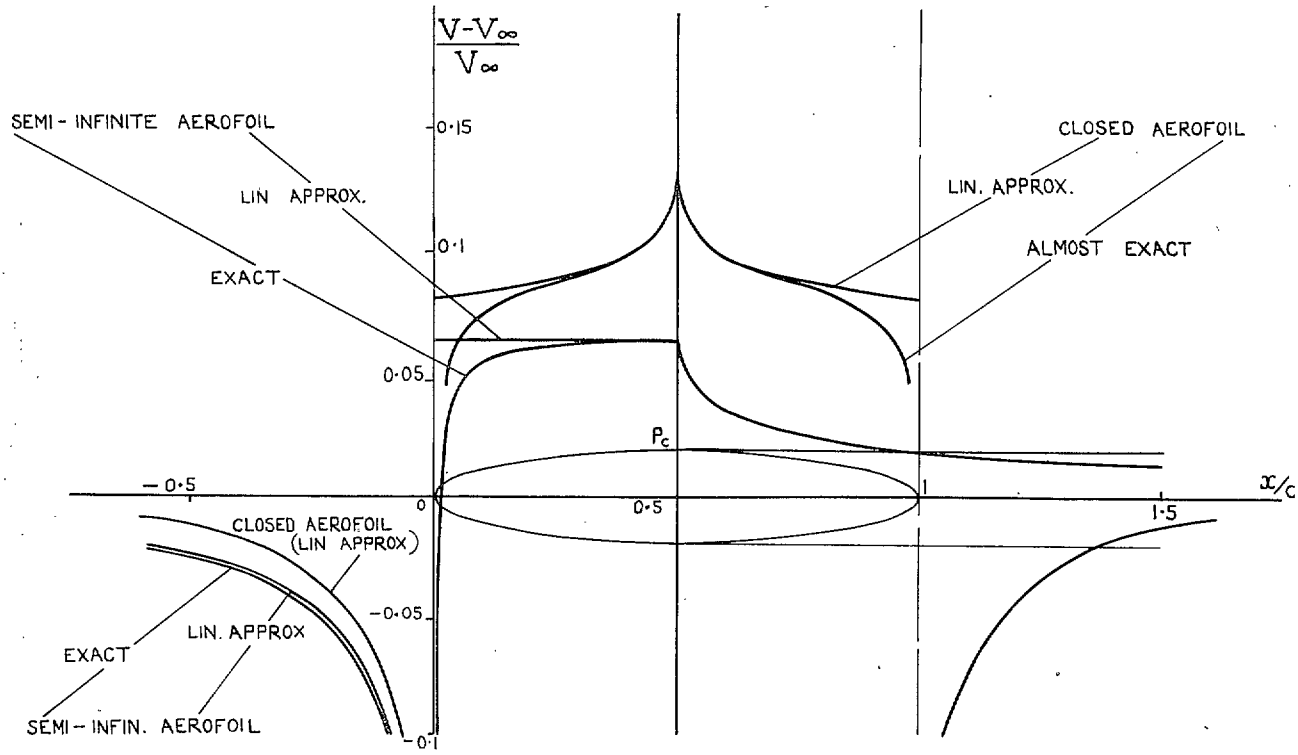

FIG. 5. Supervelocity distribution on cycloidal aerofoil, closed and semi-infinite.

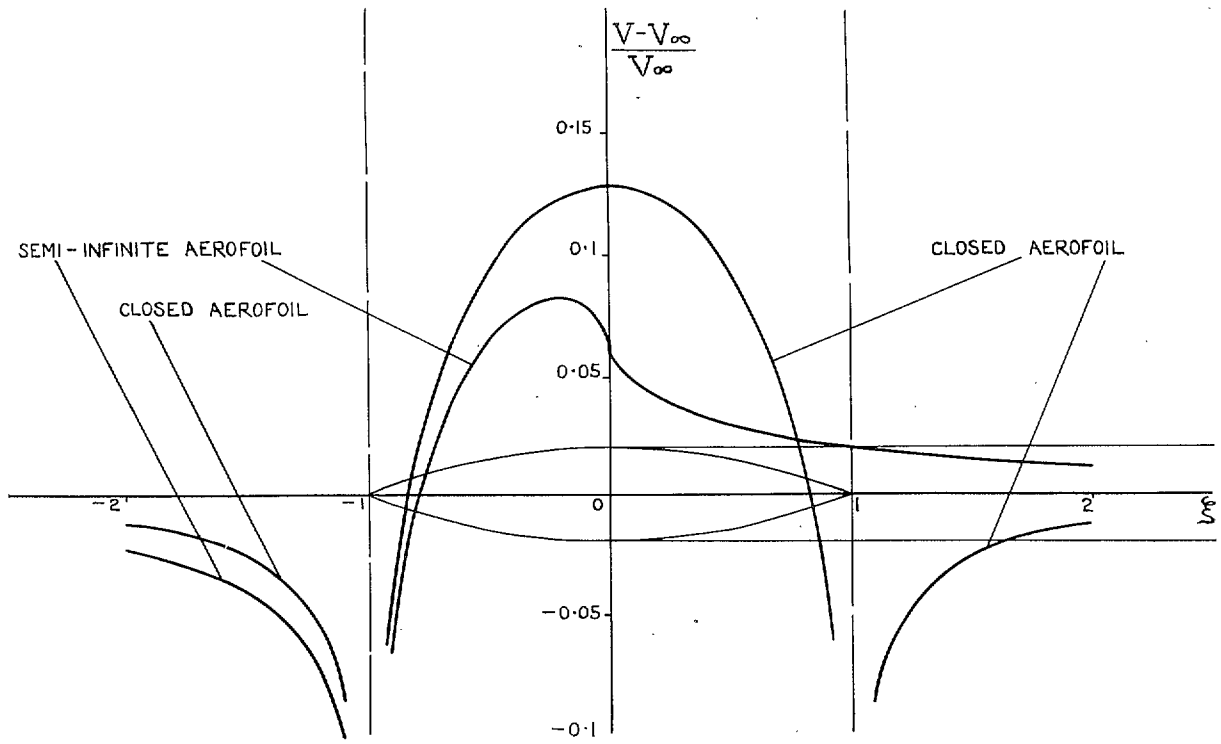

FIG. 6. Supervelocity distribution on biconvex parabolic aerofoil, closed and semi-infinite. Linear approximation.

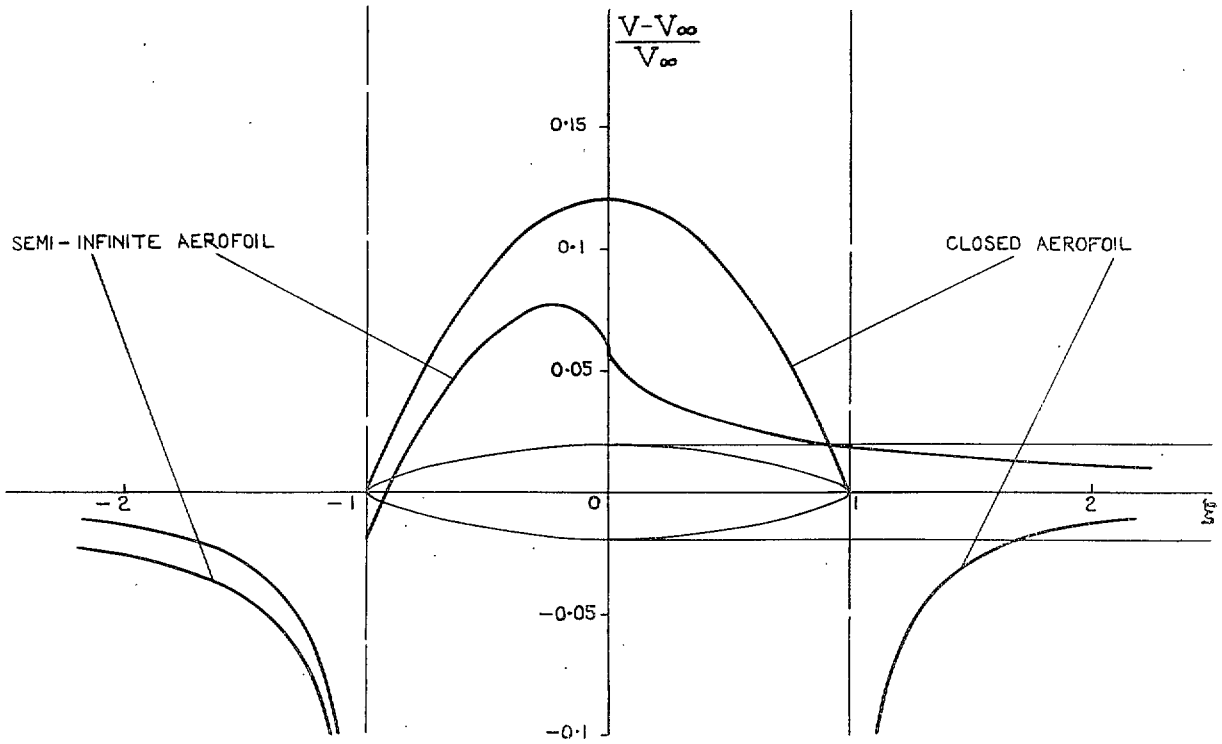

FIG. 7. Supervelocity distribution on thin-nosed oval aerofoil, closed and semi-infinite. Profile formula (6·1). $k = -0{\cdot}4$. Linear approximation.

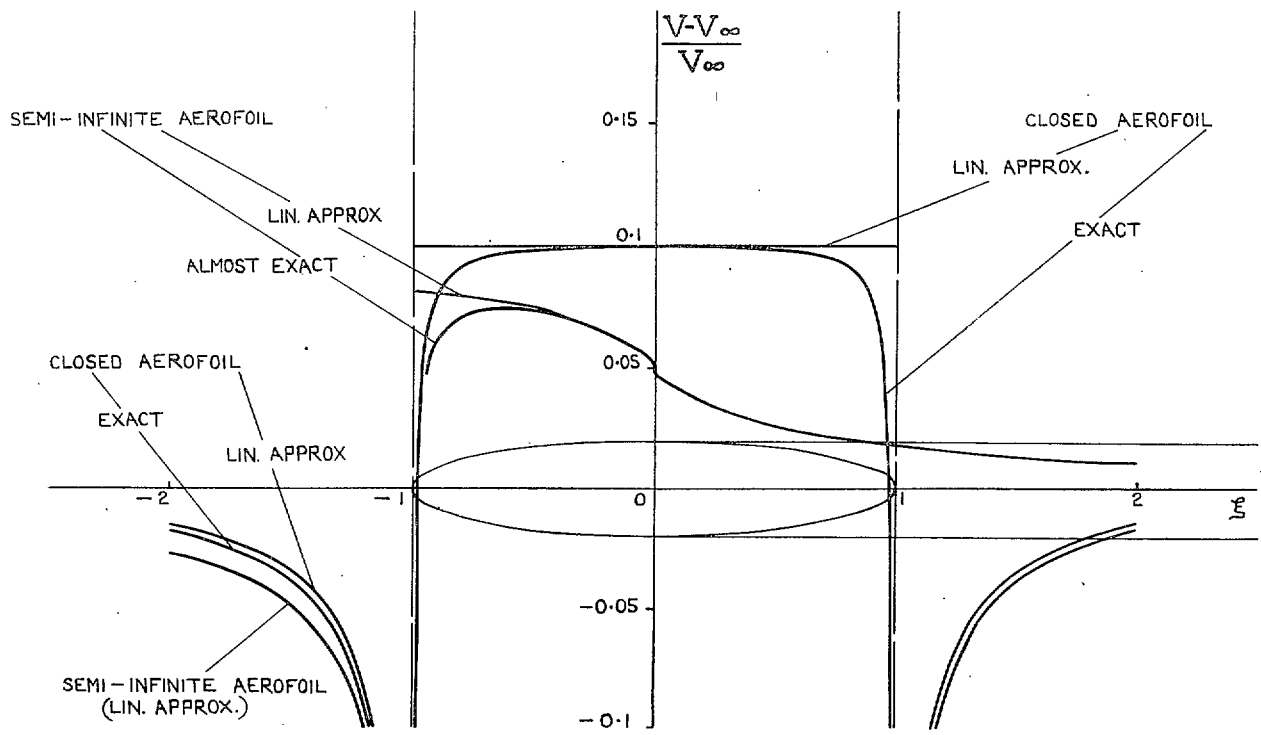

FIG. 8. Supervelocity distribution on elliptic aerofoil, closed and semi-infinite.

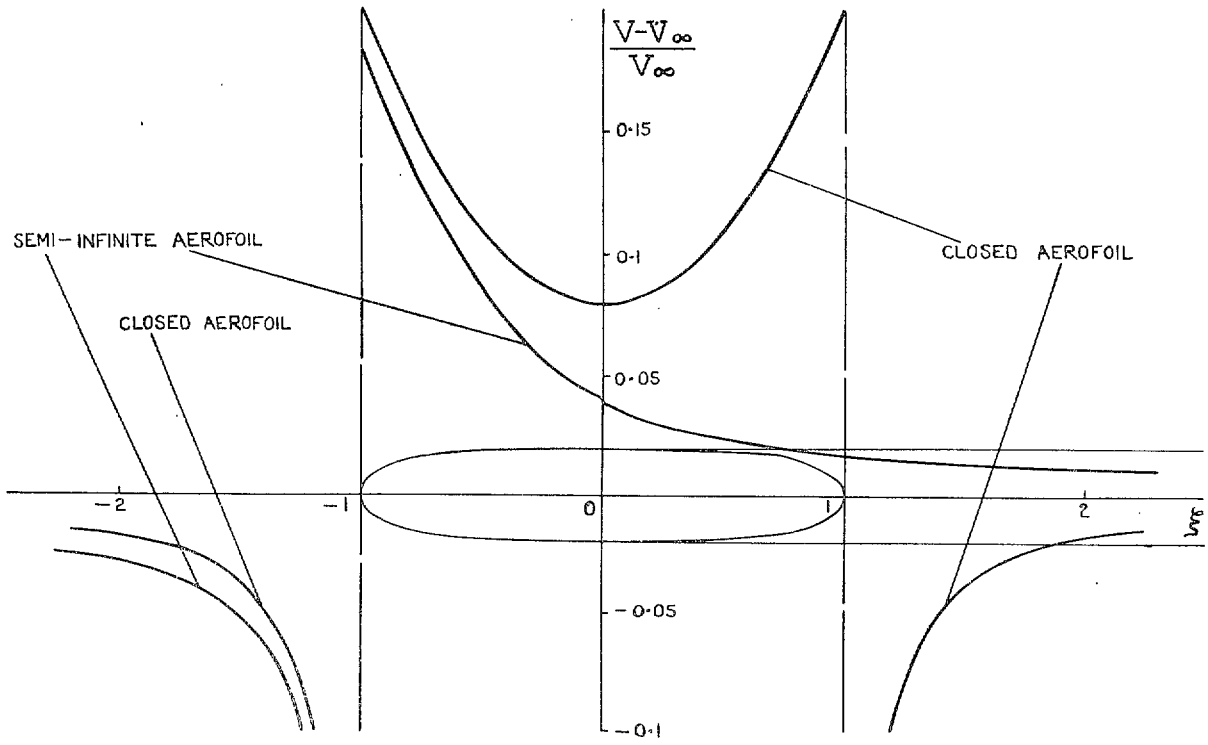

FIG. 9. Supervelocity distribution on blunt oval aerofoil, closed and semi-infinite. Profile formula (6·1). $k = +0{\cdot}4$. Linear approximation.

(4626) Wt. 20/9036 K.7 3/57 Hw.

Publications of the Aeronautical Research Council

ANNUAL TECHNICAL REPORTS OF THE AERONAUTICAL RESEARCH COUNCIL (BOUND VOLUMES)

1939 Vol. I. Aerodynamics General, Performance, Airscrews, Engines. 50*s*. (51*s*. 9*d*.).
Vol. II. Stability and Control, Flutter and Vibration, Instruments, Structures, Seaplanes, etc. 63*s*. (64*s*. 9*d*.)

1940 Aero and Hydrodynamics, Aerofoils, Airscrews, Engines, Flutter, Icing, Stability and Control Structures, and a miscellaneous section. 50*s*. (51*s*. 9*d*.)

1941 Aero and Hydrodynamics, Aerofoils, Airscrews, Engines, Flutter, Stability and Control Structures. 63*s*. (64*s*. 9*d*.)

1942 Vol. I. Aero and Hydrodynamics, Aerofoils, Airscrews, Engines. 75*s*. (76*s*. 9*d*.)
Vol. II. Noise, Parachutes, Stability and Control, Structures, Vibration, Wind Tunnels. 47*s*. 6*d*. (49*s*. 3*d*.)

1943 Vol. I. Aerodynamics, Aerofoils, Airscrews. 80*s*. (81*s*. 9*d*.)
Vol. II. Engines, Flutter, Materials, Parachutes, Performance, Stability and Control, Structures. 90*s*. (92*s*. 6*d*.)

1944 Vol. I. Aero and Hydrodynamics, Aerofoils, Aircraft, Airscrews, Controls. 84*s*. (86*s*. 3*d*.)
Vol. II. Flutter and Vibration, Materials, Miscellaneous, Navigation, Parachutes, Performance, Plates and Panels, Stability, Structures, Test Equipment, Wind Tunnels. 84*s*. (86*s*. 3*d*.)

1945 Vol. I. Aero and Hydrodynamics, Aerofoils. 130*s*. (132*s*. 6*d*.)
Vol. II. Aircraft, Airscrews, Controls. 130*s*. (132*s*. 6*d*.)
Vol. III. Flutter and Vibration, Instruments, Miscellaneous, Parachutes, Plates and Panels, Propulsion. 130*s*. (132*s*. 3*d*.)
Vol. IV. Stability, Structures, Wind Tunnels, Wind Tunnel Technique. 130*s*. (132*s*. 3*d*.)

Annual Reports of the Aeronautical Research Council—

1937 2*s*. (2*s*. 2*d*.) 1938 1*s*. 6*d*. (1*s*. 8*d*.) 1939–48 3*s*. (3*s*. 3*d*.)

Index to all Reports and Memoranda published in the Annual Technical Reports, and separately—

April, 1950 - - - - R. & M. 2600 2*s*. 6*d*. (2*s*. 8*d*.)

Author Index to all Reports and Memoranda of the Aeronautical Research Council—

1909—January, 1954 R. & M. No. 2570 15*s*. (15*s*. 6*d*.)

Indexes to the Technical Reports of the Aeronautical Research Council—

December 1, 1936—June 30, 1939	R. & M. No. 1850	1*s*. 3*d*. (1*s*. 5*d*.)
July 1, 1939—June 30, 1945	R. & M. No. 1950	1*s*. (1*s*. 2*d*.)
July 1, 1945—June 30, 1946	R. & M. No. 2050	1*s*. (1*s*. 2*d*.)
July 1, 1946—December 31, 1946	R. & M. No. 2150	1*s*. 3*d*. (1*s*. 5*d*.)
January 1, 1947—June 30, 1947	R. & M. No. 2250	1*s*. 3*d*. (1*s*. 5*d*.)

Published Reports and Memoranda of the Aeronautical Research Council—

Between Nos. 2251–2349	R. & M. No. 2350	1*s*. 9*d*. (1*s*. 11*d*.)
Between Nos. 2351–2449	R. & M. No. 2450	2*s*. (2*s*. 2*d*.)
Between Nos. 2451–2549	R. & M. No. 2550	2*s*. 6*d*. (2*s*. 8*d*.)
Between Nos. 2551–2649	R. & M. No. 2650	2*s*. 6*d*. (2*s*. 8*d*.)

Prices in brackets include postage

HER MAJESTY'S STATIONERY OFFICE

York House, Kingsway, London W.C.2; 423 Oxford Street, London W.1 (Post Orders: P.O. Box 569, London S.E.1)
13a Castle Street, Edinburgh 2; 39 King Street, Manchester 2; 2 Edmund Street, Birmingham 3; 109 St. Mary Street, Cardiff; Tower Lane, Bristol, 1; 80 Chichester Street, Belfast, *or through any bookseller.*

S.O. Code No. 23-2994